Coupling impedances of small discontinuities: Dependence on beam velocity

Sergey S. Kurennoy
Los Alamos National Laboratory, Los Alamos, New Mexico 87545, USA
(Received 22 March 2006; published 23 May 2006)

The beam coupling impedances of small discontinuities of an accelerator vacuum chamber have been calculated [e.g., Kurennoy, Gluckstern, and Stupakov, Phys. Rev. E **52**, 4354 (1995)] for ultrarelativistic beams using the Bethe diffraction theory. Here we extend the results to an arbitrary beam velocity. The vacuum chamber is assumed to have an arbitrary, but uniform along the beam path, cross section. The longitudinal and transverse coupling impedances are derived in terms of series over cross-section eigenfunctions, while the discontinuity shape enters via its polarizabilities. Simple explicit formulas for two important particular cases—circular and rectangular chamber cross sections—are presented. The impedance dependence on the beam velocity exhibits some unusual features: for example, the reactive impedance, which dominates in the ultrarelativistic limit, can vanish at a certain beam velocity, or its magnitude can exceed the ultrarelativistic value many times. In addition, we demonstrate that the same technique, the field expansion into a series of cross-section eigenfunctions, is convenient for calculating the space-charge impedance of uniform beam pipes with arbitrary cross section.

DOI: 10.1103/PhysRevSTAB.9.054201 PACS numbers: 41.75.−i, 41.20.−q

I. INTRODUCTION

A common tendency in design of modern accelerators is to minimize beam-chamber coupling impedances to avoid beam instabilities and reduce heating. Even contributions from tiny discontinuities like pumping holes have to be accounted for because of their typically large numbers. Direct numerical methods encounter difficulties in calculating the impedances of small discontinuities. The difficulties of usual time-domain methods—computing wake potentials and then finding the impedances as their Fourier transforms—are mostly technical for ultrarelativistic beams: one has to apply very fine steps in wake computations to resolve small obstacles. However, for nonultrarelativistic beams the usual numerical approach fails due to difficulty in implementing proper boundary conditions at the open ends of the beam pipe. This situation makes analytical methods especially important. A general analytical approach for calculating the beam coupling impedances of small discontinuities on the walls of an accelerator vacuum chamber has been developed in [1,2] for ultrarelativistic beams. The method is based on the Bethe theory of diffraction by small holes [3], according to which the fields diffracted by a hole can be found as those radiated by effective electric and magnetic dipoles.

The Bethe idea of effective dipoles developed in 1944 was first used to calculate the coupling impedances of pumping holes in a circular waveguide for the case of an ultrarelativistic beam in 1992 [4,5]. Bethe's theory is applicable for wavelengths large compared to the typical hole size h, and it can be used for impedance calculations when h is much smaller than the typical dimension b of the chamber cross section. Within this limitation, the theory was applied to vacuum chambers with an arbitrary simply connected cross section in [2], again for relativistic beams. The imaginary part of the impedance was shown to be proportional to the difference of hole polarizabilities $(\psi - \chi)$, where the magnetic susceptibility ψ and the electric polarizability χ are both small compared to b^3. From considerations of the energy radiated into the chamber and through the hole, the real part of the hole impedance comes out to be proportional to $(\psi^2 + \chi^2)$, being usually much smaller than the reactance. These results are not restricted to small holes, but remain valid for other small discontinuities like posts, masks, or irises, because the idea of effective polarizabilities works equally well in those cases, as was demonstrated in [6,7]. A more refined theory that takes into account the reaction of radiated waves back on the hole was developed in [1]. In the latter approach, the beam coupling impedances of a discontinuity come out as perturbative series in polarizabilities, more exactly, in small parameters ψ/b^3 and χ/b^3: the reactive impedance is the first order effect, while the real part of the impedance has the second order. Moreover, the theory [1] contains nonperturbative effects: it gives the trapped modes near the pipe cutoff frequencies due to some small discontinuities. This effect was discovered earlier using a different method [8].

In the present article we extend the analytical approach [1,2] to the case of nonultrarelativistic beams. The beam coupling impedances of a small discontinuity on the walls of a vacuum chamber with any simply connected cross section are derived for an arbitrary beam velocity $v = \beta c$. The theory gives analytical expressions for the longitudinal and transverse coupling impedances in terms of series over cross-section eigenfunctions. The shape of the discontinuity enters via its electric and magnetic polarizabilities. Previous results for ultrarelativistic beams are naturally reproduced in the limit of $\beta \to 1$. Simple explicit expressions for the impedances of nonultrarelativistic beams are

derived for circular and rectangular chamber cross sections.

One should mention a few earlier results related to the subject. The coupling impedances of a small hole in a circular beam pipe were calculated [9] for $\beta < 1$ in the form of series involving roots of Bessel functions. Closed-form expressions of the hole impedances for nonrelativistic beams in a cylindrical vacuum chamber with a circular cross section were obtained by Gluckstern *et al.* [10,11]. The longitudinal impedance of a small round hole in a circular waveguide was derived in a closed form for a beam with $\beta < 1$ and a finite transverse size in [12]. In a somewhat related paper [13], the bunch loss factors were investigated for nonultrarelativistic beams. All the results above, however, have been restricted to the particular case of an axisymmetric vacuum chamber. Our study treats a more general case of an arbitrary chamber cross section.

In addition, we show that the same technique—based on field expansions in cross-section eigenfunctions—works very efficiently for deriving the space-charge impedance of a uniform waveguide having an arbitrary cross section. A general expression is obtained that includes frequency corrections to and beam-velocity dependence of the space-charge g-factor. In the particular case of a circular cross section, the results coincide with the known ones, e.g. [11]. For a rectangular chamber, the space-charge impedance is expressed in the form of a simple series convenient for computation.

The paper is organized as follows. A general analysis of the beam fields and fields scattered by a small discontinuity in the vacuum chamber is given in Sec. II. Section III presents the derivation and results for the coupling impedances of small discontinuities. In Sec. IV the space-charge impedance of a homogeneous chamber with an arbitrary cross section is calculated. The eigenfunctions and some derivations for the two particular cases of the vacuum chamber—with a circular and rectangular cross section—are presented in the Appendices.

II. FIELDS

Let us consider an infinite cylindrical pipe with an arbitrary cross section S and perfectly conducting walls. The z axis is directed along the pipe axis, a small discontinuity (e.g., a hole) is located in the cross section $z = 0$ at the point $(\vec{b}, 0)$, and a typical hole size h satisfies $h \ll b$. The discontinuity is considered small when its size is much smaller than the wavelength of interest. To evaluate the coupling impedance, one has to calculate the fields induced in the chamber by a given current. Consider a charge q that moves on or parallel to the chamber axis with velocity $v = \beta c$. A rigid bunch is usually assumed for wake or impedance calculations. It is convenient to choose a ''pancake'' charge distribution such that the charge and current densities are given by

$$\begin{aligned} \rho(\vec{r}, z; t) &= q f(\vec{r}) \delta(z - \beta c t), \\ \vec{j}(\vec{r}, z; t) &= q \beta c f(\vec{r}) \delta(z - \beta c t) \hat{z}, \end{aligned} \tag{1}$$

where $f(\vec{r})$ is a normalized transverse charge distribution, $\int_S d\vec{r} f(\vec{r}) = 1$, $\delta(x)$ is Dirac's delta function, and $\hat{z}$ is a unit vector in the z-direction. The distribution (1) includes two particular cases that are especially convenient in calculations: a point charge with the transverse offset $\vec{s}$ from the axis, when $f(\vec{r}) = \delta(\vec{r} - \vec{s})$, and a thin axisymmetric ring of radius a with $f(\vec{r}) = \delta(r - a)/(2\pi a)$. In frequency domain, omitting factor $\exp(-i\omega t)$, the current density harmonic (1) becomes

$$\vec{j}(\vec{r}, z; \omega) = q f(\vec{r}) e^{i\omega z/(\beta c)} \hat{z}. \tag{2}$$

This harmonic corresponds to the space harmonic $k = \omega/(\beta c)$. From Maxwells's equations in frequency domain follow the wave equations for harmonics of the beam field components:

$$\begin{aligned} (\nabla^2 + \partial_z^2) E_z + \omega^2/c^2 E_z &= i\omega\mu_0/(\beta^2\gamma^2) j_z, \\ (\nabla^2 + \partial_z^2) \vec{E}_\perp + \omega^2/c^2 \vec{E}_\perp &= 1/(\varepsilon_0 \beta c) \vec{\nabla} j_z, \\ (\nabla^2 + \partial_z^2) \vec{H}_\perp + \omega^2/c^2 \vec{H}_\perp &= -(\hat{z} \times \vec{\nabla}) j_z. \end{aligned} \tag{3}$$

Here all quantities are functions of $(\vec{r}, z; \omega)$, $\vec{\nabla}$ is the two-dimensional (2D) gradient in plane S, $\partial_z \equiv \partial/\partial z$, $\gamma = 1/\sqrt{1 - \beta^2}$, and j_z is defined from Eq. (2). The longitudinal component of the magnetic field is not excited by the current (1), so that $H_z = 0$.

Let us now introduce eigenvalues k_g^2 and orthonormalized eigenfunctions (EFs) $e_g(\vec{r})$ of the Dirichlet boundary problem in S:

$$(\nabla^2 + k_g^2) e_g = 0; \qquad e_g|_{\partial S} = 0, \tag{4}$$

where $g = \{n, m\}$ is a generalized 2D index. Since EFs form a complete set in S, the transverse dependence of solutions to Eqs. (3) can be found as a series in EFs. Obviously, the solutions should depend on the longitudinal coordinate as $\exp(i\omega z/\beta c)$. Then the field harmonics $\vec{E}, \vec{H}$ produced by the charge distribution (1) at the location $(\vec{b}, z)$ on the chamber wall without hole can be expressed in terms of EFs (4) as

$$\begin{aligned} E_\nu(\vec{b}, z; \omega) &= Z_0 H_\tau(\vec{b}, z; \omega)/\beta \\ &= -\frac{Z_0 q}{\beta} \exp\left(i\frac{\omega z}{\beta c}\right) \sum_g \frac{f_g \nabla_\nu e_g(\vec{b})}{k_g^2 + \kappa^2}, \end{aligned} \tag{5}$$

where it was convenient to introduce $\kappa \equiv \omega/(\beta\gamma c)$. Here $Z_0 = \sqrt{\mu_0/\varepsilon_0} = 120\pi$ Ohms is the impedance of free space, $\hat{\nu}$ means an outward normal unit vector, $\hat{\tau}$ is a unit vector tangent to the boundary ∂S of the chamber cross section S, $\nabla_\nu \equiv \vec{\nabla} \cdot \hat{\nu}$, and $\{\hat{\nu}, \hat{\tau}, \hat{z}\}$ form a right-handed basis. In Eq. (5) f_g are the coefficients of EF expansion

$f(\vec{r}) = \sum_g f_g e_g(\vec{r})$; they are given by $f_g = \int_S d\vec{r} f(\vec{r}) e_g(\vec{r})$. For the case of a point charge with the transverse offset $\vec{s}$ from the axis, we have $f_g = e_g(\vec{s})$. The eigenvalues and EFs for particular cross sections are given in the Appendices.

In a similar way, the longitudinal component of the electric field produced by the current (1) as a function of the transverse coordinates $\vec{r}$ is

$$E_z(\vec{r}, z; \omega) = -i \frac{\omega}{\beta c} \frac{Z_0 q}{\beta \gamma^2} e^{i\omega z/(\beta c)} \sum_g \frac{f_g e_g(\vec{r})}{k_g^2 + \kappa^2}. \quad (6)$$

Obviously, E_z vanishes at the chamber wall because of the Dirichlet boundary conditions (BCs) for EFs (4). The transverse fields on the wall (5) are not zero since the series (5) includes the gradients of EFs and $\nabla_\nu e_g(\vec{b}) \neq 0$.

Note that one could use EFs different from EFs (4) to calculate the transverse magnetic field $\vec{H}_\perp$. A convenient choice would be to use EFs $h_g(\vec{r})$ of the Neumann boundary problem, which differs from (4) by the BCs, $\nabla_\nu h_g|_{\partial S} = 0$. However, we chose to relate $\vec{H}_\perp$ to the transverse electric field $\vec{E}_\perp$ directly from the Maxwell equations. For the harmonic $k = \omega/(\beta c)$, one gets $Z_0 \hat{z} \times \vec{H}_\perp = -\beta \vec{E}_\perp$, from which the first line in Eqs. (5) follows immediately.

One more remark about Eqs. (5) is worthwhile. Since the lowest eigenvalue k_g is of the order of $1/b$, in the long-wavelength limit, $\kappa b = \omega b/(\beta\gamma c) \ll 1$, the sums in Eqs. (5) and (6) become independent of frequency and of β. The only remaining dependence on the beam velocity $E_\nu \propto 1/\beta$ seems counterintuitive: one would expect $H_\tau \propto \beta$. The apparent contradiction disappears as soon as we recall that Eqs. (5) give the field harmonics with wave number $k = \omega/(\beta c)$, not the beam fields in time domain.

Now we have to calculate the fields scattered into the vacuum chamber by the discontinuity. According to the Bethe theory, at distances l such that $h \ll l \ll b$, the fields radiated by the discontinuity (hole) into the pipe are equal to those produced by effective dipoles [3,14]

$$P_\nu = -\chi \varepsilon_0 E_\nu^h/2; \qquad M_\tau = (\psi_{\tau\tau} H_\tau^h + \psi_{\tau z} H_z^h)/2; \qquad M_z = (\psi_{z\tau} H_\tau^h + \psi_{zz} H_z^h)/2, \quad (7)$$

where superscript h means that the beam fields (5) are taken at the hole location $(\vec{b}, 0)$. Polarizabilities ψ, χ are related to the effective ones α_e, α_m used in [4,14] as $\alpha_e = -\chi/2$ and $\alpha_m = \psi/2$, so that for a circular hole of radius h in a thin wall $\psi = 8h^3/3$ and $\chi = 4h^3/3$ [3]. In general, ψ is a symmetric 2D-tensor, which can be diagonalized. If the discontinuity is symmetric, and its symmetry axis is parallel to $\hat{z}$, the skew terms vanish, i.e. $\psi_{\tau z} = \psi_{z\tau} = 0$. In a more general case of a nonzero tilt angle α between the major symmetry axis and $\hat{z}$,

$$\begin{aligned} \psi_{\tau\tau} &= \psi_\perp \cos^2\alpha + \psi_\parallel \sin^2\alpha, \\ \psi_{\tau z} &= \psi_{z\tau} = (\psi_\parallel - \psi_\perp) \sin\alpha \cos\alpha, \\ \psi_{zz} &= \psi_\perp \sin^2\alpha + \psi_\parallel \cos^2\alpha, \end{aligned} \quad (8)$$

where $\psi_\parallel$ is the longitudinal magnetic susceptibility (for the external magnetic field along the major axis), and $\psi_\perp$ is the transverse one (the field is transverse to the major axis of the hole). Formulas for polarizabilities of various discontinuities are collected in the handbook [15], see also Ref. [16].

It is important to emphasize that we can use the static values of the polarizabilities [15,16] in Eqs. (7) only when the beam fields (5) do not change significantly from one point of the discontinuity to another, i.e., when

$$\frac{\omega h}{\beta c} \ll 1. \quad (9)$$

Physically, it means that the wavelength of interest $\lambda = 2\pi/k = 2\pi\beta c/\omega$ is much larger than the discontinuity size h, so that all discontinuity points are excited and radiate with approximately the same phase. Equation (9) gives the applicability condition for our results. For most small discontinuities, it is satisfied at frequencies of practical interest. The frequency range can be extended even further if we include frequency corrections to the static polarizabilities. Such corrections were calculated for a few types of discontinuities, e.g., for elliptical holes [17].

When the effective dipoles are obtained by substituting beam fields (5) into Eqs. (7), one can calculate the scattered fields as a sum of waveguide eigenmodes excited in the chamber by the dipoles, and find the impedance. This approach has been carried out for a circular pipe in [4], and for an arbitrary chamber in [2], for ultrarelativistic beams. The fields radiated into the chamber by the effective dipoles (7) can be found as a series in TM- and TE eigenmodes [14]:

$$\vec{F} = \sum_g [A_g^+ \vec{F}_g^{(E)+} \theta(z) + A_g^- \vec{F}_g^{(E)-} \theta(-z)] + \sum_g [B_g^+ \vec{F}_g^{(H)+} \theta(z) + B_g^- \vec{F}_g^{(H)-} \theta(-z)], \quad (10)$$

where $\vec{F}$ means either $\vec{E}$ or $\vec{H}$, $g = \{n, m\}$ is a 2D index; superscripts $\pm$ denote waves radiated, respectively, in the positive (+, $z > 0$) or negative ($-$, $z < 0$) direction, and $\theta(z)$ is the Heaviside step function. The fields $F_g^{(E)}$ of the gth TM-eigenmode in Eq. (10) are expressed [14] in terms of EFs (4)

$$\begin{aligned} E_z^\mp &= k_g^2 e_g \exp(\pm\Gamma_g z); \\ H_z^\mp &= 0; \\ \vec{E}_t^\mp &= \pm\Gamma_g \vec{\nabla} e_g \exp(\pm\Gamma_g z); \\ \vec{H}_t^\mp &= i\omega\varepsilon_0 \hat{z} \times \vec{\nabla} e_g \exp(\pm\Gamma_g z), \end{aligned} \quad (11)$$

where propagation factors $\Gamma_g = (k_g^2 - \omega^2/c^2)^{1/2}$ should be replaced by $-i\beta_g$ with $\beta_g = (\omega^2/c^2 - k_g^2)^{1/2}$ for $\omega/c > k_g$. For given values of dipoles (7) the coefficients $A_g^{\pm}$ can be found [2,4] using the Lorentz reciprocity theorem

$$A_g^{\pm} = a_g M_\tau \pm b_g P_\nu, \tag{12}$$

with

$$a_g = -\frac{i\omega\mu_0}{2\Gamma_g k_g^2}\nabla_\nu e_g^h; \qquad b_g = \frac{1}{2\varepsilon_0 k_g^2}\nabla_\nu e_g^h. \tag{13}$$

Here the EFs are taken at the hole location $\vec{b}$ on the wall, $e_g^h \equiv e_g(\vec{b})$.

Similarly, the fields $F_g^{(H)}$ of the TE_g-eigenmode in Eq. (10) are

$$\begin{aligned} H_z^{\mp} &= k_g'^2 h_g \exp(\pm\Gamma_g' z);\\ E_z^{\mp} &= 0;\\ \vec{H}_t^{\mp} &= \pm\Gamma_g'\vec{\nabla}h_g \exp(\pm\Gamma_g' z);\\ \vec{E}_t^{\mp} &= -i\omega\mu_0\hat{z}\times\vec{\nabla}h_g \exp(\pm\Gamma_g' z), \end{aligned} \tag{14}$$

with propagation factors $\Gamma_g' = (k_g'^2 - \omega^2/c^2)^{1/2}$ replaced by $-i\beta_g' = -i(\omega^2/c^2 - k_g'^2)^{1/2}$ when $\omega/c > k_g'$. Here EFs h_g satisfy the boundary problem (4) with the Neumann boundary condition, $\nabla_\nu h_g|_{\partial S} = 0$, and $k_g'^2$ are corresponding eigenvalues, see the Appendices. The TE-mode excitation coefficients in the expansion (10) for the radiated fields are

$$B_g^{\pm} = \pm c_g M_\tau + d_g P_\nu + q_g M_z, \tag{15}$$

where

$$\begin{aligned} c_g &= \frac{1}{2k_g'^2}\nabla_\tau h_g^h; \qquad q_g = \frac{1}{2\Gamma_g'} h_g^h;\\ d_g &= -\frac{i\omega}{2\Gamma_g' k_g'^2}\nabla_\tau h_g^h. \end{aligned} \tag{16}$$

From Eqs. (10)–(16), using the effective dipoles (7) induced on the discontinuity by the beam fields (5), we find the fields scattered by the discontinuity into the vacuum chamber. Note that the dependence on the beam velocity enters explicitly only in Eq. (5). Now we proceed with the impedance calculation.

III. BEAM COUPLING IMPEDANCE OF A SMALL DISCONTINUITY

A. Longitudinal impedance

In a general case, the longitudinal impedance is defined (e.g., [18,19]) as an integral along the vacuum chamber of the (synchronous with the beam) harmonic of the longitudinal electric field E_z created in the chamber by the leading charge (1) divided by the amplitude of the corresponding harmonic of the beam current (1). The field E_z should be taken at the longitudinal position of a unit test charge that follows the leading one with the same velocity, and should also be integrated over the test-charge transverse distribution $t(\vec{r})$. This leads to the formula

$$Z(\omega) = -\frac{1}{q}\int_{-\infty}^{\infty} dz e^{-i[(\omega z)/(\beta c)]}\int_S d\vec{r}\, t(\vec{r}) E_z(\vec{r}, z; \omega), \tag{17}$$

where normalization $\int_S d\vec{r}\, t(\vec{r}) = 1$ is assumed. Note that the longitudinal field E_z includes both the beam field (6) and the scattered field (10) produced by the discontinuity. The first one is related to the space-charge impedance and vanishes at $\gamma \to \infty$; we will consider it in Sec. IV. Here we include into E_z only the discontinuity contribution. All z-dependence in Eq. (10) is in the exponents, so integrating over z is straightforward. For transverse integration, we expand the test-charge transverse distribution $t(\vec{r})$ in EFs as $t(\vec{r}) = \sum_g t_g e_g(\vec{r})$, where $t_g = \int_S d\vec{r}\, t(\vec{r}) e_g(\vec{r})$. The result is

$$Z(\omega) = i\frac{\omega}{qc}\left(Z_0 M_\tau + \frac{1}{\beta}\frac{P_\nu}{\varepsilon_0}\right)\sum_g \frac{t_g \nabla_\nu e_g^h}{k_g^2 + \kappa^2}, \tag{18}$$

where we again use variable $\kappa = \omega/(\beta\gamma c)$ introduced earlier in Eq. (5). Substituting the dipole expressions (7), where the beam fields (5) are taken at the hole location $(\vec{b}, 0)$, leads to

$$Z(\omega) = -iZ_0\frac{\omega}{c}\frac{\psi_{\tau\tau} - \chi/\beta^2}{2}\sum_g \frac{f_g \nabla_\nu e_g^h}{k_g^2 + \kappa^2}\sum_g \frac{t_g \nabla_\nu e_g^h}{k_g^2 + \kappa^2}. \tag{19}$$

It is convenient to introduce the following notation:

$$e_\nu(f;\kappa) \equiv -\sum_g \frac{f_g \nabla_\nu e_g^h}{k_g^2 + \kappa^2}. \tag{20}$$

Comparing to Eqs. (5), one can see that $e_\nu(f;\kappa)$ is related to the transverse harmonics of the beam field at the hole location as

$$e_\nu(f;\kappa) = \frac{E_\nu(\vec{b}, 0; \omega)\beta}{Z_0 q} = \frac{H_\tau(\vec{b}, 0; \omega)}{q}. \tag{21}$$

As was already mentioned in Sect. II, the lowest eigenvalue k_g is of the order of $1/b$. Therefore, for $\omega b/(\beta\gamma c) = \kappa b \ll 1$, the normalized transverse field Eq. (20) becomes frequency and velocity independent:

$$e_\nu(f;0) = -\sum_g f_g k_g^{-2}\nabla_\nu e_g^h. \tag{22}$$

The condition $\omega b/(\beta\gamma c) \ll 1$ includes two cases: (i) ultrarelativistic limit, $\gamma \to \infty$; and (ii) long-wavelength (or low-frequency) limit, when the wavelength $\lambda = 2\pi/k = 2\pi\beta c/\omega$ is large compared to the typical cross-section size b. Equation (22) has a simple physical interpretation. It

gives a solution for a 2D electrostatic field created on the chamber wall in the cross section S by a uniform in z charge, equal to ε_0 per unit length of z, that has the transverse distribution $f(\vec{r})$. From the Gauss law, $e_\nu(f)$ satisfies the normalization condition

$$\oint_{\partial S} dl e_\nu(f;0) = 1, \tag{23}$$

where integration goes along the cross-section boundary ∂S. For a simple particular case of a circular cross section with radius b, and an axisymmetric charge distribution $f(\vec{r}) = f(r)$—it includes an on-axis point charge—Eq. (23) by itself provides the solution, due to the problem symmetry: $e_\nu(f;0) = 1/(2\pi b)$, cf. [2,4].

When the test-charge distribution is identical to that of the leading charge, $t(\vec{r}) = f(\vec{r})$, Eq. (19) gives the discontinuity impedance for the given transverse charge distribution $f(\vec{r})$ of the beam as

$$Z(\omega) = -iZ_0 \frac{\omega}{c} [e_\nu(f;\kappa)]^2 \left(\alpha_m + \frac{\alpha_e}{\beta^2}\right), \tag{24}$$

where we use the effective polarizabilities $\alpha_m = \psi_{\tau\tau}/2$ and $\alpha_e = -\chi/2$, and $e_\nu(f;\kappa)$ is defined by (20).

The generalized longitudinal impedance is usually defined with the leading and test point charges having different transverse displacement from the chamber axis, $\vec{s}$ and $\vec{t}$, respectively [1,18]. In that case, Eq. (19) can be rewritten as

$$Z(\vec{s},\vec{t};\omega) = -iZ_0 \frac{\omega}{c} e_\nu(\vec{s};\kappa) e_\nu(\vec{t};\kappa) \left(\alpha_m + \frac{\alpha_e}{\beta^2}\right), \tag{25}$$

where

$$e_\nu(\vec{r};\kappa) \equiv -\sum_g \frac{e_g(\vec{r}) \nabla_\nu e_g^h}{k_g^2 + \kappa^2}. \tag{26}$$

The last expression follows from Eq. (20) because $f_g = e_g(\vec{r})$ for a point charge with transverse displacement $\vec{r}$ from the chamber axis. The impedance (25) includes higher multipole longitudinal impedances. The usual monopole longitudinal impedance is obtained from Eq. (25) when the charges are on axis, $s \to 0$ and $t \to 0$:

$$Z(\omega) = -iZ_0 \frac{\omega}{c} e_\nu^2(0;\kappa) \left(\alpha_m + \frac{\alpha_e}{\beta^2}\right). \tag{27}$$

In the ultrarelativistic limit, $\beta \to 1$ and $\gamma \to \infty$, the normalized field $e_\nu(0;\kappa)$ becomes

$$\tilde{e}_\nu \equiv -\sum_g k_g^{-2} e_g(0) \nabla_\nu e_g^h, \tag{28}$$

cf. (22), and Eq. (27) coincides with the known result for the impedance of a small discontinuity [1,2].

For some particular cases of simple cross sections S, one can obtain explicit expressions of the normalized field (20) and the longitudinal impedance (27). The derivation is presented in the Appendices for circular and rectangular cross sections. For a circular cross section of radius b, (27) takes form

$$Z(\omega) = -iZ_0 \frac{\omega}{c} \frac{\alpha_m + \beta^{-2}\alpha_e}{4\pi^2 b^2} [I_0(\kappa b)]^{-2}, \tag{29}$$

which coincides, up to notations, with the result in [10]. Here $I_0(x)$ is the modified Bessel function of the first kind.

For a rectangular cross section $a \times b$, assuming that the hole is located on the side wall at $x = a$, $y = y_h$, the longitudinal impedance (27) is

$$Z(\omega) = -iZ_0 \frac{\omega}{c} \frac{\alpha_m + \beta^{-2}\alpha_e}{b^2} \times \left[\sum_{p=0}^{\infty} \frac{(-1)^p \sin[\pi(2p+1)y_h/b]}{\cosh(\pi u_{2p+1}/2)}\right]^2, \tag{30}$$

where $u_m = a\sqrt{m^2/b^2 + \kappa^2/\pi^2}$. In the ultrarelativistic limit, Eq. (30) coincides with the result in [1], see Appendix B for detail.

For the case of an axisymmetric small obstacle on the wall of a circular beam pipe—like a small enlargement (cavity) or an iris—the longitudinal impedance turns out to be very similar to Eq. (27):

$$\begin{aligned} Z(\omega) &= -iZ_0 \frac{\omega}{c} e_\nu^2(0;\kappa) 2\pi b \left(\tilde{\alpha}_m + \frac{\tilde{\alpha}_e}{\beta^2}\right) \\ &= -iZ_0 \frac{\omega}{c} \frac{\tilde{\alpha}_m + \beta^{-2}\tilde{\alpha}_e}{2\pi b} [I_0(\kappa b)]^{-2}, \end{aligned} \tag{31}$$

where the effective polarizabilities $\tilde{\alpha}_m$ and $\tilde{\alpha}_m$ are now defined per unit length of the circumference $2\pi b$ of the chamber cross section (circle) S. In transition from the first line in Eq. (31) to the second one, we used the known expression for $e_\nu(0;\kappa)$ in a circular cross section, cf. Eq. (29). Essentially, for an axisymmetric discontinuity $\alpha_{m,e}$ in Eqs. (27) and (29) are replaced by $2\pi b\tilde{\alpha}_{m,e}$. In the ultrarelativistic limit, $\beta \to 1$, Eq. (31) coincides with the previous results [6,7]. It is worth mentioning that, if an axisymmetric enlargement has area A of the longitudinal cross section, its magnetic polarizability is $\tilde{\alpha}_m = A$, while for an axisymmetric protrusion (iris) of the same cross-section area $\tilde{\alpha}_m = -A$. The electric polarizability $\tilde{\alpha}_e$ can be found by solving a 2D electrostatic problem, see examples in [6,7,16]. It is positive for protrusions and negative for enlargements, so that in both cases $\tilde{\alpha}_m$ and $\tilde{\alpha}_e$ have opposite signs.

The longitudinal impedances (25), (27), and also (31), depend on the beam velocity in two ways: via $e_\nu(\vec{s};\kappa)$ and in the combination of polarizabilities $(\alpha_m + \alpha_e/\beta^2)$. The first dependence enters via the parameter $\kappa b = \omega b/(\beta\gamma c)$, as one can see from Eqs. (26) and (29)–(31). For $\kappa b \ll 1$ the factor $e_\nu^2(\vec{s};\kappa)$ is close to its ultrarelativistic limit, while at $\kappa b > 1$ it decreases exponentially to zero. We should emphasize that for $\beta < 1$ the monopole longitudinal impedance depends on the beam position in

the chamber cross section, unlike its ultrarelativistic counterpart [19]. For a circular cross section this dependence takes a particularly simple form as an additional factor of $I_0^2(\kappa t)$ in (29) and (31), where t is the beam transverse displacement from the chamber axis, see Eq. (A3) in Appendix A.

In the combination $\alpha_m + \alpha_e/\beta^2$ the electric contribution is enhanced as the beam velocity decreases. This sum (more exactly, this difference, because α_m and α_e always have opposite signs) can either vanish for some values of β, or become much larger than its ultrarelativistic limit $\alpha_m + \alpha_e$. It vanishes when $0 < \beta = \sqrt{-\alpha_e/\alpha_m} < 1$. We should note that such a situation occurs only for discontinuities like holes or chamber enlargements (small cavities), since for them $\alpha_m > |\alpha_e|$ [2]. For instance, a circular hole of radius h in a thin wall has $\alpha_m = 4h^3/3$ and $\alpha_e = -2h^3/3$, so that $\sqrt{-\alpha_e/\alpha_m} = 1/\sqrt{2}$. The impedance (27) of the hole, which is inductive for relativistic beams, changes its sign for $\beta < 1/\sqrt{2}$ becoming a "negative inductance." On the other hand, for protrusions and irises the impedance remains inductive for any beam velocity because of $\alpha_e > |\alpha_m|$, cf. [6,7]. As a simple example, a semispherical protrusion (bump) of radius a on the wall has polarizabilities $\alpha_e = 2\pi a^3$ and $\alpha_m = -\pi a^3$ [7].

For all small discontinuities the impedance vanishes at very slow beam velocities, when $\beta \to 0$, since the fast decrease of the factor $e_\nu^2(\vec{s};\kappa)$ suppresses the growth due to α_e/β^2. This behavior is illustrated in Fig. 1 for a hole and in Fig. 2 for a protrusion, both in a circular cylindrical chamber with the radius b of its cross section. For other cross sections the impedance behavior is similar: the impedance magnitude can exceed the ultrarelativistic value many times. In fact, the ratio $Z(\beta)/Z(1)$ for $\omega b/c = 0.1$ in Fig. 1 reaches -83.3 at $\beta = 0.062$, and in Fig. 2 its maximum is 167.5, well outside the shown range. The

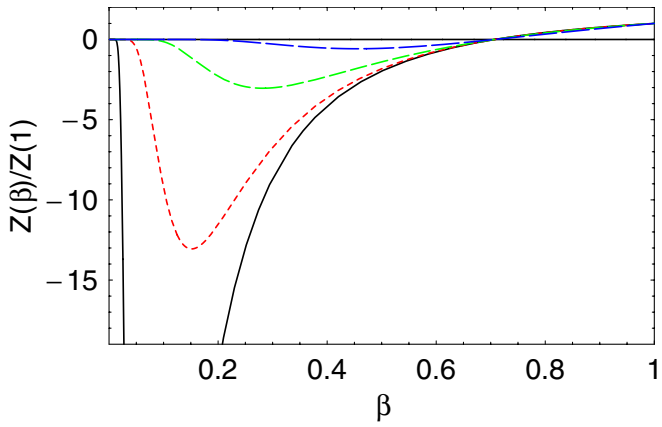

FIG. 1. (Color) The ratio of the longitudinal impedance (29) to its relativistic value for a circular hole in a round pipe versus $\beta = v/c$ for $\omega b/c = 0.1, 0.25, 0.5, 1$ (solid, short-dashed, dashed, and long-dashed curves).

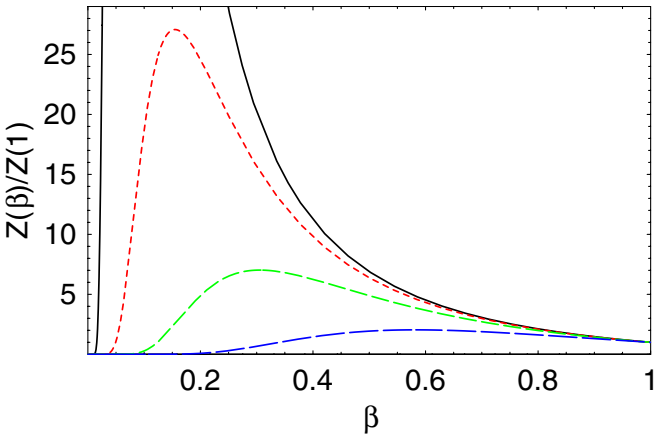

FIG. 2. (Color) The same, for a small semispherical protrusion.

extremes become even larger for lower frequencies. It is worthwhile to note that the results in Figs. 1 and 2 are independent of the discontinuity size h provided that $h \ll b$ and, of course, the applicability condition (9) is satisfied, i.e. $\omega h \ll \beta c$.

Another interesting example of β-dependence is for long elliptic slots parallel to the chamber axis. If the ellipse semiaxes w, l satisfy $w \ll l \ll b$, the leading terms ($\propto w^2 l$) of the static polarizabilities α_m and α_e for a thin wall cancel each other [2,4] in the ultrarelativistic limit:

$$\alpha_m + \alpha_e \approx \frac{\pi w^2 l}{3}\left[\frac{w^2}{l^2}\left(\ln\frac{4l}{w} - 1\right) - \frac{1}{5}\left(\frac{\omega l}{c}\right)^2\right]. \qquad (32)$$

Here the first term in the square brackets comes from the next-to-leading order static contributions, and the second one is the leading frequency correction [17]. Even though Eq. (32) was derived assuming $\omega l \ll c$, for narrow long slots with $w \ll l$ the frequency correction can be significant. For $\beta < 1$ there is no cancellation of the leading static terms. The frequency corrections to the magnetic and electric polarizabilities [17] also contribute differently to the modified sum, all of which results in

$$\alpha_m + \frac{\alpha_e}{\beta^2} \approx \frac{\pi w^2 l}{3}\left[\frac{w^2}{l^2}\left(\frac{1+\beta^2}{2\beta^2}\ln\frac{4l}{w} - \frac{1}{4\beta^2} - \frac{3}{4}\right) - \frac{1}{5}\left(2 - \frac{1}{\beta^2}\right)\left(\frac{\omega l}{\beta c}\right)^2 - \frac{1}{\beta^2\gamma^2}\right]. \qquad (33)$$

The correspondence between Eqs. (33) and (32) is clear: the first term in the square brackets of (33) is the next-to-leading order static term, the second one gives the frequency correction, while the last term—absent in (32)—is the leading static contribution for $\beta < 1$. One should recall that Eq. (33) is valid within the parameter range given by the applicability condition (9), which in this case means $\omega l \ll \beta c$. The frequency correction in (33) vanishes when $\beta = 1/\sqrt{2}$ and changes sign at lower beam velocities. For small β Eq. (33) has an opposite sign and larger magnitude compared to its relativistic limit (32).

The longitudinal impedance in Eqs. (24)–(27) is purely inductive. In the sense of a perturbative expansion in the small parameters $|\alpha_m|/b^3 \ll 1$ and $|\alpha_e|/b^3 \ll 1$, it is the first-order term. In Ref. [1] higher-order terms were studied by taking into account radiative corrections to the fields near the discontinuity. The second-order term has both an imaginary and real part; the last one appears only at frequencies above the chamber cutoff. The real part of the impedance includes contributions from only a finite number of the eigenmodes propagating in the chamber at a given frequency, i.e., those with $k_g < \omega/c$ or $k_g' < \omega/c$. The dependence of ReZ on frequency is complicated: it has sharp peaks near the cutoffs of all propagating eigenmodes of the chamber, but increases on average with the frequency increase. Well above the chamber cutoff, i.e., when $\omega b/c \gg 1$ [still $\omega h/(\beta c) \ll 1$ to justify the Bethe approach], this averaged dependence can be derived in exactly the same way as in [1] for ultrarelativistic beams. The result is

$$\mathrm{Re}\, Z(\omega) = \frac{Z_0 \omega^4}{3\pi c^4} e_\nu^2(0;\kappa)\left(\alpha_m^2 + \alpha_{ms}^2 + \frac{\alpha_e^2}{\beta^2}\right), \qquad (34)$$

where $\alpha_{ms} \equiv \psi_{\tau z}/2$, cf. Eqs. (7) and (8). Alternatively, the same answer can be obtained by calculating the energy radiated by the effective dipoles (7) into a half-space. The physical reason for this coincidence is that at frequencies well above the cutoff they radiate into the waveguide the same energy as into an open half-space.

We conclude this subsection by emphasizing that Eqs. (25)–(31) give the leading, imaginary part of the longitudinal impedance for nonultrarelativistic beams within the frequency range defined by the applicability condition (9). For most small discontinuities, it includes frequencies well above the beam pipe cutoff. As was already mentioned in discussing the real part of the impedance, in well conducting beam pipes with holes or enlargements there will be narrow resonances due to the trapped modes near the cutoff frequencies of all propagating modes [8]. These resonances modify both the real and imaginary part of the impedance given by formulas above, by adding sharp peaks near the cutoff frequencies. The shunt impedances of the trapped-mode resonances are proportional to $\alpha_m^3/(b^8\delta)$ [1,8], where δ is the skin depth, and depend on the beam velocity as β^4, see [13] for details.

B. Transverse impedance

Since we are interested in the dipole transverse impedance, it is convenient to consider the excitation by a dipole: two point charges with the opposite signs displaced from the chamber axis by $\vec{s}$ and $-\vec{s}$, correspondingly, instead of Eq. (1), moving at velocity βc along the axis. Such a change would modify the expression (25) for the longitudinal impedance replacing $e_\nu(\vec{s};\kappa)$ by $e_\nu^{\mathrm{dip}}(0;\kappa) = \vec{s}\cdot\vec{\nabla}e_\nu(0;\kappa)$, which is the second (dipole) term of its Taylor expansion, with $e_\nu(0;\kappa)$ being the first (monopole) one. After normalizing the excitation to the unit transverse beam displacement (dividing by s), we integrate the synchronous harmonic of the transverse force acting on a test charge displaced from the axis by $\vec{t}$, and then divide by the harmonic amplitude of the dipole moment creating the deflecting force:

$$\vec{Z}_\perp(\omega) = -\frac{i}{qs}\int_{-\infty}^{\infty} dz \exp\left(-i\frac{\omega z}{\beta c}\right)[\vec{E}_\perp(\vec{t},z;\omega) + Z_0\beta\hat{z}\times\vec{H}_\perp(\vec{t},z;\omega)]. \qquad (35)$$

where the usual definition of the dipole transverse impedance assumes the limit of $t \to s \to 0$, e.g. [19] or [18]. The integration result includes contributions from both TM- and TE-modes excited by the effective dipoles in the beam pipe, unlike the expression for the longitudinal impedance (25), where only TM-modes contribute.

There is an alternative way to find the transverse impedance. Since we already have expression (25) for the generalized longitudinal impedance $Z(\vec{s},\vec{t};\omega)$, we can apply the Panofsky-Wenzel theorem, e.g., in [19]. According to the theorem, the transverse impedance can be derived as

$$\vec{Z}_\perp(\vec{s},\vec{t};\omega) = \frac{\beta c}{\omega s}\vec{\nabla}_t Z(\vec{s},\vec{t};\omega), \qquad (36)$$

where the longitudinal impedance is calculated with the dipole excitation as discussed above. If we follow this way, which is simpler in our case, the result will include only TM-mode contributions, or, in other words, the EFs of (4), since only they enter Eq. (25) for the longitudinal impedance. We used the relations between the transverse components of the beam fields, cf. Eq. (5), to prove that the two results obtained are equivalent. One should remark that definition (35) sometimes includes an extra factor $1/\beta$, e.g., in [18]. For consistency with the relation (36), here we use the transverse-impedance definition without that extra factor, i.e., Eq. (35).

The final expression for the transverse dipole impedance of a discontinuity is

$$\vec{Z}_\perp(\omega) = -iZ_0\beta\left(\alpha_m + \frac{\alpha_e}{\beta^2}\right)[\hat{s}\cdot\vec{d}(\kappa)]\vec{d}(\kappa), \qquad (37)$$

where $\hat{s} = \vec{s}/s$ is a unit vector in the direction of the beam deflection from the chamber axis, and

$$\vec{d}(\kappa) \equiv \vec{\nabla}e_\nu(0;\kappa) = -\sum_g \frac{\vec{\nabla}e_g(0)\nabla_\nu e_g^h}{k_g^2 + \kappa^2}. \qquad (38)$$

The impedance dependence on the discontinuity shape is obviously the same as for the longitudinal impedance. The direction of the vector of the transverse impedance (37) gives the direction of the deflecting force acting on a displaced beam. As one can see from Eq. (37), this direction is defined by vector $\vec{d}$, Eq. (38), while the force magnitude varies depending on the relative direction of

the beam displacement $\vec{s}$ with respect to $\vec{d}$ via the scalar product $\hat{s} \cdot \vec{d}$.

For a circular beam pipe, the transverse impedance (37) can be written, making use of Eq. (A5) of Appendix A, simply as

$$\vec{Z}_\perp(\omega) = -iZ_0\beta \frac{\alpha_m + \beta^{-2}\alpha_e}{\pi^2 b^4}\left[\frac{\kappa b}{2I_1(\kappa b)}\right]^2 (\hat{s}\cdot\hat{h})\hat{h}, \tag{39}$$

where $\hat{h} = \vec{b}/b$ is a unit vector in the chamber cross section S directed from the axis to the hole (discontinuity). In this case, one can rewrite the dot product in a more conventional form, $\hat{s}\cdot\hat{h} = \cos(\varphi_s - \varphi_h)$, where φ_s is the azimuthal angle of the beam position in the cross-section plane, and φ_h is the azimuthal angle in the direction to the hole. Therefore, the deflecting force in the circular pipe is directed to (or opposite to) the discontinuity, and its magnitude depends on the angle between the hole and the beam transverse displacement, as was pointed out already in the relativistic case [4]. Equation (39) agrees, up to notations, with the result obtained in [10].

In a general case, it is sometimes convenient to rewrite the dipole transverse impedance (37) as

$$\vec{Z}_\perp(\omega) = -iZ_0\beta\left(\alpha_m + \frac{\alpha_e}{\beta^2}\right) d^2(\kappa)\hat{d}\cos(\varphi_s - \varphi_d). \tag{40}$$

In particular, this form is more convenient for the rectangular chamber. Here $d = \sqrt{d_x^2 + d_y^2}$, where x, y are the horizontal and vertical coordinates in the chamber cross section S, and d_x and d_y are projections of $\vec{d}$, cf. Appendix B; $\varphi_s = \varphi_t$ is again the azimuthal angle of the beam position in the cross-section plane; $\hat{d} = \vec{d}/d$ is a unit vector in this plane in the direction of $\vec{d}$, and φ_d is the corresponding azimuthal angle. Obviously, $d_x = d\cos\varphi_d$ and $d_y = d\sin\varphi_d$. It is seen from Eq. (40) that the angle φ_d shows the direction of the transverse-impedance vector $\vec{Z}_\perp$ and, therefore, of the beam-deflecting force. Moreover, the magnitude of $Z_\perp$ is maximal when the beam is deflected along this direction and vanishes when the beam offset is perpendicular to it. For a circular pipe, $\varphi_d = \varphi_h$, as was discussed above. For a general cross section, this is not the case even in the relativistic limit; see [2] for rectangular and elliptic chambers. As an illustration, in Fig. 3 we plot the relation between φ_d and φ_h for a square chamber for a few different values of parameter $\kappa b = \omega b/(\beta\gamma c)$. The case $\kappa b = 0$ corresponds to the relativistic (or low-frequency) limit; as κb increases, the difference between φ_d and φ_h becomes smaller.

In Fig. 4, the behavior of $d(\kappa)$ in Eq. (40) is illustrated for a square cross section of the vacuum chamber. This function is given by Eq. (B6) in Appendix B; for plotting $d(\kappa)$ is multiplied by ab to make it dimensionless. For comparison, the same plot shows a similar dependence for the circular cross section, see Eq. (39). Figure 4 demonstrates also the impedance dependence on the position of the discontinuity on the chamber wall: $y_h/b = 0.5$ corresponds to the middle of the wall, 0.75 is one quarter from the corner, and 0.9 is close to the corner. Figures 3 and 4, as well as Figs. 1 and 2, were produced using MATHEMATICA [20]. It takes less than ten terms in the series (B6) and (B3) to get a very accurate answer for the sum, which is not surprising since the 10th term in (B3) is of the order of $O(e^{-30}) = O(10^{-13})$. However, even with hundreds of terms MATHEMATICA gives the results almost as quickly as those involving modified Bessel functions for the circular pipe in Figs. 1 and 2.

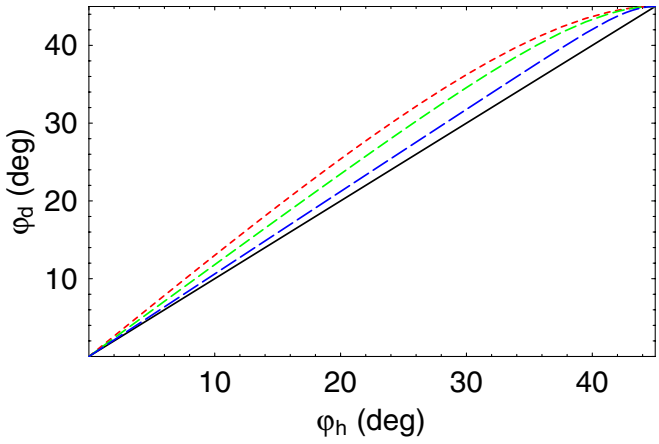

FIG. 3. (Color) Direction φ_d of the transverse impedance (40) versus hole position on the side wall of a square chamber for $\omega b/(\pi\beta\gamma c) = 0, 3, 10$ (short-dashed, dashed, and long-dashed curves). The solid line is for a circular pipe.

One should remind that the impedance magnitude decreases even faster with the frequency increase for a fixed β than shown in Fig. 4, since $Z_\perp \propto d^2$. The full

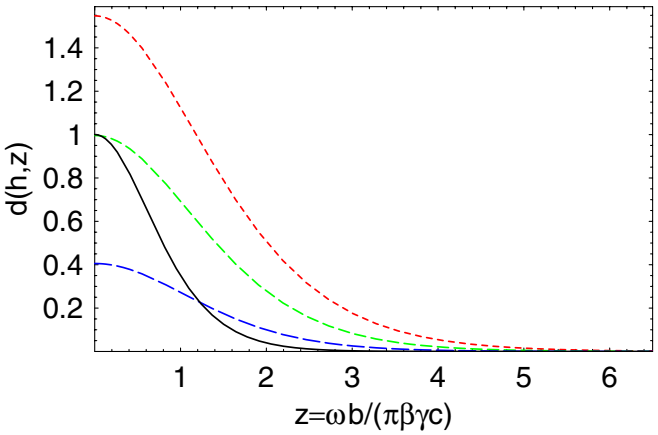

FIG. 4. (Color) Normalized magnitude of function d in Eq. (40) versus $\kappa b/\pi$ for three hole positions $h = y_h/b = 0.5, 0.75, 0.9$ on the side wall of a square chamber (short-dashed, dashed, and long-dashed curves). The solid line shows for comparison $\kappa b/2/I_1(\kappa b)$ from Eq. (39).

β-dependence of the transverse impedance includes, of course, the shape factor $\beta\alpha_m + \alpha_e/\beta$; overall, it is similar to that of the longitudinal impedance illustrated in Figs. 1 and 2.

IV. SPACE-CHARGE IMPEDANCE

We will show in this section that the same approach as above—based on field expansions in cross-section eigenfunctions—works equally well for calculating the space-charge impedance of a uniform waveguide with an arbitrary simply connected cross section. While this subject seems to be somewhat off topic for the present paper, the result comes as a by-product of the considerations in the previous sections. The synchronous harmonic of the longitudinal beam field produced in a uniform beam pipe with the cross section S by the current (2) is given by Eq. (6). Using the impedance definition (17) with the finite integration length L and assuming the same transverse charge distribution for the test charge as for the source, $t(\vec{r}) = f(\vec{r})$, we obtain the space-charge longitudinal impedance per unit length of the chamber

$$\frac{Z^{sc}(\omega)}{L} = i\frac{\omega}{c}\frac{Z_0}{\beta^2\gamma^2}\sum_g \frac{f_g^2}{k_g^2 + \kappa^2} \tag{41}$$

for a beam with the transverse charge distribution $f(\vec{r})$. The space-charge impedance (41) is expressed in terms of eigenvalues k_g of the boundary problem (4) and the expansion coefficients f_g of the charge distribution in EFs (4), $f_g = \int_S d\vec{r} f(\vec{r}) e_g(\vec{r})$. Every term of the series in Eq. (41) is positive, so that the space-charge impedance always remains a "negative inductance." It is important to emphasize that the dependence on the beam-charge distribution is an essential feature of the space-charge impedance. For example, one cannot use a pencil beam (point charge) in (41): the space-charge impedance diverges as the beam transverse size vanishes, e.g. [19]. On the contrary, the geometrical impedances discussed in the previous sections are generally independent of the beam properties, at least in the relativistic limit, and for that reason they are usually calculated in the simplest way, that is with an on-axis pencil beam.

Let us compare Eq. (41) with the conventional form of the space-charge impedance in the long-wavelength approximation, $\kappa b \ll 1$,

$$\frac{Z^{sc}(\omega)}{L} = i\frac{\omega}{c}\frac{Z_0}{\beta^2\gamma^2}\frac{1}{2\pi}g_L, \tag{42}$$

where g_L is called the longitudinal g-factor, e.g. [19,21]. One can conclude that the sum in (41) is proportional to the g-factor:

$$S(f;\kappa) \equiv \sum_g \frac{f_g^2}{k_g^2 + \kappa^2} = \frac{1}{2\pi}g_L(\kappa), \tag{43}$$

which now depends on frequency and beam velocity, in addition to its familiar dependence on the beam-charge distribution. The usual value of g-factor is obtained as the limit at $\kappa \to 0$, i.e. $g_L = g_L(0)$. Using a term-by-term consideration of series (43), it is easy to prove that g-factor is positive, $g_L(\kappa) > 0$, and that frequency corrections reduce its value: $g_L(\kappa) < g_L(0)$.

In the well-studied particular case of a circular cross section, we consider the beam in the form of a thin axisymmetric ring of radius a, $f(\vec{r}) = \delta(r - a)/(2\pi a)$. The summation is performed in Appendix A, and the result

$$S(f;\kappa) = \frac{I_0(\kappa a)}{2\pi}\left[K_0(\kappa a) - I_0(\kappa a)\frac{K_0(\kappa b)}{I_0(\kappa b)}\right] \tag{44}$$

coincides with the familiar one, e.g., in [11]. In the long-wavelength limit $\kappa b \ll 1$, Eq. (44) gives the well-known g-factor of a hollow beam $S = \ln(b/a)/(2\pi)$.

For a rectangular chamber of width a and height b, to simplify calculations, we choose somewhat exotic beam-charge distribution: a centered hollow beam with a similar rectangular profile ζa, ζb, where the beam-size scale $0 < \zeta < 1$. Even in a simpler case of a square chamber, $a = b$, the space-charge factor (43) of the square hollow beam $\zeta a \times \zeta a$ is given by a rather long expression (see Appendix B):

$$\begin{aligned} S(f;\kappa) = {} & \frac{2}{\pi^3\zeta^2}\sum_{p=0}^{\infty}\frac{\sin[\pi(2p+1)\zeta/2]}{2p+1} \\ & \times \frac{\sinh[\pi u_{2p+1}(1-\zeta)/2]}{u_{2p+1}\cosh(\pi u_{2p+1}/2)} \\ & \times \left\{\frac{\sin[\pi(2p+1)\zeta/2]}{2p+1}\cosh(\pi u_{2p+1}\zeta/2)\right. \\ & \left. + \frac{\cos[\pi(2p+1)\zeta/2]}{u_{2p+1}}\sinh(\pi u_{2p+1}\zeta/2)\right\}, \end{aligned} \tag{45}$$

where $u_n = \sqrt{n^2 + (\kappa a/\pi)^2}$. We found analytically that in the relativistic (or long-wavelength) limit, $\kappa a \to 0$, the leading term of Eq. (45) is $\ln(1/\zeta)/(2\pi)$, exactly the same as in the case of a circular pipe above. The series (45) converges slower than the series in (30) or (B6), so up to 2500 terms were included in our MATHEMATICA computations for this series. Still it took only a couple of minutes of CPU time on a PC to produce Figs. 5 and 6. They illustrate the behavior of $S(f;\kappa)$ (45) as a function of the frequency and beam size. It is interesting that the sum $S(f, 0)$ (relativistic or static limit) is very close to its ln asymptotic even for the beam size as large as one half of the pipe size, $\zeta = 0.5$, cf. Fig. 5. The frequency dependence of the space-charge impedance (more precisely, of the g-factor) plotted in Fig. 6 is weaker than that for the impedances of small discontinuities in Fig. 4.

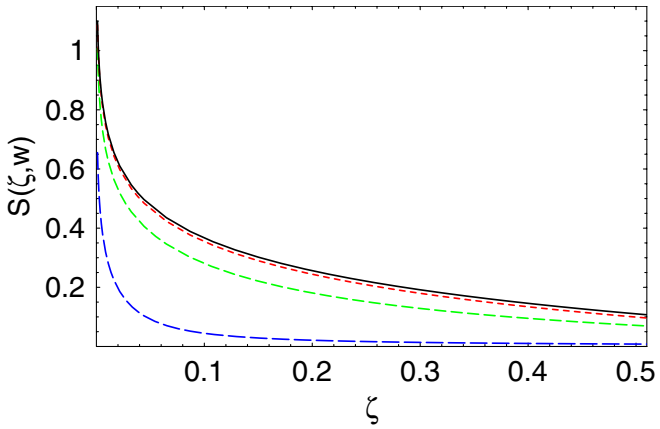

FIG. 5. (Color) Function S (45) for a square chamber versus the ratio ζ of the beam size to the chamber size a at three different values of $w = \kappa a/\pi = 0, 1, 10$ (short-dashed, dashed, and long-dashed curves). The solid curve shows the analytical relativistic limit $\ln(1/\zeta)/(2\pi)$.

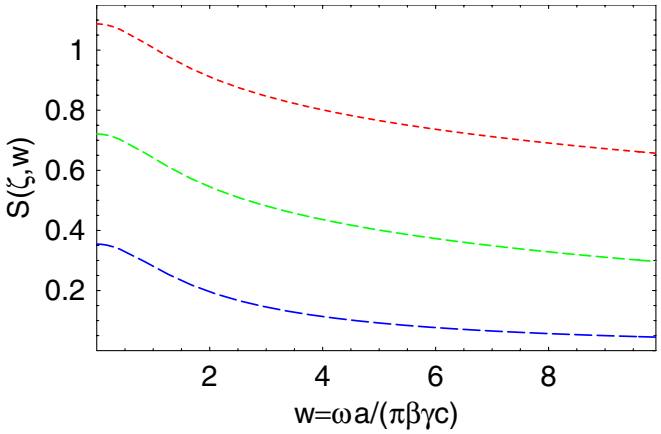

FIG. 6. (Color) The same versus $w = \kappa a/\pi$ for three different beam sizes ζa, $\zeta = 0.001, 0.01, 0.1$ (short-dashed, dashed, and long-dashed curves).

V. DISCUSSION

The approach of Refs. [1,2], where the impedances of small discontinuities were calculated in the ultrarelativistic case, was extended to the beams with an arbitrary velocity and transverse charge distribution. The analytical approach presented above provides a general picture of the coupling impedances for small discontinuities of the vacuum chamber with an arbitrary cross section in a wide frequency range, up to frequencies well above the cutoff. The upper limit on the frequency is imposed by the applicability of the Bethe theory: the wavelength must be large compared to the typical size h of the discontinuity. This applicability condition requires $\omega h/(\beta c) \ll 1$, cf. the discussion of Eq. (9). For a given frequency and beam velocity, it limits the size of discontinuities for which our formulas work. On the other hand, given the frequency and the discontinuity size, this requirement restricts from below the range of beam velocities at which the results are applicable.

We concentrated mostly on the leading (imaginary) part of the impedances created by small discontinuities. In a general case, it was shown that the coupling impedances of small discontinuities depend on the beam velocity in two ways: first, through the combination of polarizabilities $(\alpha_m + \alpha_e/\beta^2)$, and second, via the parameter $\kappa = \omega/(\beta\gamma c)$ that enters into the factors $e_\nu(\kappa)$ for the longitudinal impedance, see Eqs. (29)–(31), and $d(\kappa)$ for the transverse one, Eqs. (37)–(41). The first factor contains all the impedance dependence on the discontinuity shape, while the second one accounts for effects of the chamber cross section and the discontinuity location on the cross-section boundary. The second factor behaves in the same way for various cross sections: it decreases from its value at $\kappa = 0$, which can be interpreted as either the ultrarelativistic or long-wavelength limit, as κ increases. The decrease rate depends to some extent on the cross-section shape and the discontinuity position, but for $\kappa b > 1$ the decrease is fast (exponential), as evidenced by Eqs. (29), (31), and (39), as well as by Fig. 4. The overall impedance dependence on the beam velocity for small discontinuities was discussed in Sec. III. The most interesting feature is that the impedance magnitude for some $\beta < 1$ can exceed its relativistic value many times, see Figs. 1 and 2.

The impedances for the circular and rectangular cross sections of the vacuum chamber were derived from the obtained formulas by substituting corresponding EFs. The expressions can be useful for calculating the beam coupling impedances in particle accelerators with nonultrarelativistic beams. For the circular pipe our results agree with those obtained earlier for $\beta < 1$ in [10,11]. In a similar way, the results for an elliptic chamber can be expressed in terms of Mathieu functions; it seems unlikely, however, that such a series would be convenient for calculations. For a complicated cross-section shape the relativistic-limit factors $e_\nu(0)$ and $d(0)$ can be found numerically by solving a 2D electrostatic problem, see [2] for an elliptical pipe. Applying the results obtained above, one can give then an impedance estimate for a given beam velocity in such a chamber.

We also demonstrated that the same technique—using the field expansion into a series of cross-section eigenfunctions—works well for calculating the space-charge impedance of a uniform vacuum chamber with an arbitrary cross section. A generalized expression $g(\kappa)$ for the longitudinal space-charge g-factor is derived. It depends on the beam velocity and on frequency, in addition to the usual dependence on the transverse beam-charge distribution. The generalized g-factor $g(\kappa)$ decreases monotonically as κ increases: $g(0) \geq g(\kappa) > 0$. It is worthwhile to notice that the long-wavelength (or relativistic) limiting value $g(0)$ can be calculated numerically even for very complicated vacuum chambers, e.g., those with screening wires and ceramic insertions [21].

APPENDIX A: CIRCULAR CHAMBER

For a circular cross section of radius b the eigenvalues $k_{nm} = \mu_{nm}/b$, where μ_{nm} is mth zero of the Bessel function $J_n(x)$, $n = 0, 1, 2, \ldots$, and $m = 1, 2, \ldots$. The normalized EFs in circular coordinates (r, φ) are

$$e_{nm}(r, \varphi) = \frac{J_n(k_{nm}r)}{\sqrt{N^E_{nm}}} \begin{Bmatrix} \cos n\varphi \\ \sin n\varphi \end{Bmatrix}, \tag{A1}$$

with $N^E_{nm} = \pi b^2 \epsilon_n J^2_{n+1}(\mu_{nm})/2$, where $\epsilon_0 = 2$ and $\epsilon_n = 1$ for $n \neq 0$. For TE-modes, $k'_{nm} = \mu'_{nm}/b$ with $J'_n(\mu'_{nm}) = 0$, and

$$h_{nm}(r, \varphi) = \frac{J_n(k'_{nm}r)}{\sqrt{N^H_{nm}}} \begin{Bmatrix} \cos n\varphi \\ \sin n\varphi \end{Bmatrix}, \tag{A2}$$

where $N^H_{nm} = \pi b^2 \epsilon_n (1 - n^2/\mu'^2_{nm}) J^2_n(\mu'_{nm})/2$.

The series (26) for the circular cross section can be easily summed

$$\begin{aligned} e_\nu(\vec{r}; \kappa) &= \frac{2}{\pi b} \sum_{n=0}^{\infty} \frac{\cos[n(\varphi - \varphi_h)]}{\epsilon_n} \\ &\quad \times \sum_{m=1}^{\infty} \frac{\mu_{nm} J_n(\mu_{nm} r/b)}{J_{n+1}(\mu_{nm})[\mu^2_{nm} + (\kappa b)^2]} \\ &= \frac{1}{\pi b} \sum_{n=0}^{\infty} \frac{\cos[n(\varphi - \varphi_h)]}{\epsilon_n} \frac{I_n(\kappa r)}{I_n(\kappa b)}, \end{aligned} \tag{A3}$$

where $I_n(x)$ are the modified Bessel functions, and $\kappa = \omega/(\beta\gamma c)$. For the last step in the above equation the summation was performed using formulas from [22]. The impedances of a hole in a circular pipe for $\beta < 1$ were derived in [9] in terms of sums similar to that in the second line of Eq. (A3). The resulting sum (A3) is essentially a multipole expansion. In the limit of an on-axis beam, $r \to 0$, it becomes simply

$$e_\nu(0; \kappa) = \frac{1}{2\pi b} \frac{1}{I_0(\kappa b)}. \tag{A4}$$

The result simplifies even further in the relativistic limit. For $\gamma \to \infty$, $e_\nu(0; \kappa) \to e_\nu(0; 0) \equiv \tilde{e}_\nu$ and becomes $\tilde{e}_\nu = 1/(2\pi b)$, which also follows from the Gauss law. Then the inductive impedance (27) takes an especially simple form derived earlier in Refs. [4,5].

For calculating the transverse impedance, we need to find the gradient of the field (A3) at the origin, cf. definition (38). Only the second term ($n = 1$) in the series (A3) gives a nonvanishing contribution when $r \to 0$:

$$\vec{d}(\kappa) = \vec{\nabla} e_\nu(0; \kappa) = \frac{1}{\pi b^2} \frac{\kappa b}{2 I_1(\kappa b)} \hat{h}, \tag{A5}$$

where $\hat{h} = \vec{b}/b$ is a unit vector in the chamber cross section S directed from the axis to the hole (discontinuity). In the limit of $\gamma \to \infty$, Eq. (A5) simplifies to $\vec{d} = \hat{h}/(\pi b^2)$, in agreement with [4,5].

For space-charge impedance calculations, we consider the beam-charge distribution in the form of a thin axisymmetric ring of radius a, $f(\vec{r}) = \delta(r - a)/(2\pi a)$. Then the EF expansion coefficients are

$$f_{nm} = \delta_{n0} \frac{J_0(\mu_{0m} a/b)}{\sqrt{N^E_{0m}}} \begin{Bmatrix} 1 \\ 0 \end{Bmatrix}, \tag{A6}$$

where δ_{nm} is the Kronecker symbol. The sum (43) becomes

$$\begin{aligned} S(f; \kappa) &= \frac{1}{\pi} \sum_{m=1}^{\infty} \frac{J^2_0(\mu_{0m} a/b)}{J^2_1(\mu_{0m})(\mu^2_{0m} + \kappa^2 b^2)} \\ &= \frac{I_0(\kappa a)}{2\pi} \left[K_0(\kappa a) - I_0(\kappa a) \frac{K_0(\kappa b)}{I_0(\kappa b)} \right], \end{aligned} \tag{A7}$$

where formulas [22] were applied.

APPENDIX B: RECTANGULAR CHAMBER

For a rectangular chamber of width a and height b the eigenvalues are $k_{nm} = \pi\sqrt{n^2/a^2 + m^2/b^2}$ with $n, m = 1, 2, \ldots$, and the normalized EFs are

$$e_{nm}(x, y) = \frac{2}{\sqrt{ab}} \sin\frac{\pi n x}{a} \sin\frac{\pi m y}{b}, \tag{B1}$$

with $0 \le x \le a$ and $0 \le y \le b$. Let a hole be located in the side wall at $x = a, y = y_h$. Assuming the beam displacement $\vec{s}$ from the chamber axis $(a/2, b/2)$, we can perform one summation in Eq. (26) to reduce the double sum into a fast-converging series

$$\begin{aligned} e_\nu(\vec{s}; \kappa) &= \frac{2}{b} \sum_{m=1}^{\infty} \sin\left[\pi m \left(\frac{1}{2} + \frac{s_y}{b} \right) \right] \sin\left(\frac{\pi m y_h}{b} \right) \\ &\quad \times \frac{\sinh[\pi u_m (1/2 + s_x/a)]}{\sinh(\pi u_m)}, \end{aligned} \tag{B2}$$

where $u_m = \sqrt{m^2 a^2/b^2 + \kappa^2 a^2/\pi^2}$. For an on-axis beam, $s \to 0$, it can be simplified to

$$e_\nu(0; \kappa) = \frac{1}{b} \sum_{p=0}^{\infty} \frac{(-1)^p \sin[\pi(2p+1) y_h/b]}{\cosh[\pi u_{2p+1}/2]}. \tag{B3}$$

In the relativistic limit, $\beta \to 1$, $\gamma \to \infty$, Eq. (B3) becomes

$$e_\nu(0; \kappa) \to e_\nu(0; 0) \equiv \tilde{e}_\nu = \frac{1}{b} \Sigma\left(\frac{a}{b}, \frac{y_h}{b} \right), \tag{B4}$$

where

$$\Sigma(u, v) = \sum_{p=0}^{\infty} \frac{(-1)^p \sin[\pi(2p+1)v]}{\cosh[\pi(2p+1)u/2]}, \tag{B5}$$

which coincides with the result [1] for the rectangular chamber. For some particular values of υ, e.g. $\upsilon = 1/2$, the sum $\Sigma(u, \upsilon)$ can be expressed in terms of the complete elliptic integrals; in general, it is easy to calculate the series numerically because of its fast (exponential) convergence. Its behavior versus υ for different values of the aspect ratio u was plotted in Ref. [2].

The gradient of the field (B2) at the origin is required for calculating the transverse impedance. In the Cartesian coordinates $\{x, y\}$, it is

$$\vec{d}(\kappa) \equiv \{d_x, d_y\} = \vec{\nabla} e_\nu(0; \kappa) = \frac{\pi}{ab}\left\{\sum_{p=0}^{\infty}(-1)^p \frac{u_{2p+1}\sin[\pi(2p+1)y_h/b]}{\sinh(\pi u_{2p+1}/2)}; \frac{a}{b}\sum_{p=0}^{\infty}(-1)^p \frac{2p\sin(2\pi p y_h/b)}{\cosh(\pi u_{2p}/2)}\right\}. \tag{B6}$$

In the ultrarelativistic limit $u_m \to ma/b$, and gradient (B6) becomes frequency independent:

$$\vec{d}(0) = \frac{\pi}{b^2}\left\{\sum_{p=0}^{\infty}(-1)^p \frac{(2p+1)\sin[\pi(2p+1)y_h/b]}{\sinh[\pi(p+1/2)a/b]}; \sum_{p=0}^{\infty}(-1)^p \frac{2p\sin(2\pi p y_h/b)}{\cosh(\pi p a/b)}\right\}. \tag{B7}$$

For calculating the space-charge impedance of a centered rectangular hollow beam $\zeta a \times \zeta b$ in the beam pipe with rectangular cross section $a \times b$, the EF-expansion coefficients are

$$f_{nm} = \frac{4\sin(\pi n/2)\sin(\pi m/2)}{\pi^2\zeta(a+b)\sqrt{ab}}\left(\frac{a}{n}\sin\frac{\pi n\zeta}{2}\cos\frac{\pi m\zeta}{2} + \frac{b}{m}\cos\frac{\pi n\zeta}{2}\cos\frac{\pi m\zeta}{2}\right). \tag{B8}$$

Substituting f_{nm} into Eq. (43) and performing one summation to reduce the resulting double sum to a series leads to Eq. (45).

[1] S. S. Kurennoy, R. L. Gluckstern, and G. V. Stupakov, Phys. Rev. E **52**, 4354 (1995).

[2] S. S. Kurennoy, in Proceedings of the Third EPAC, Berlin, 1992, p. 871; more details in IHEP (Protvino) Report No. 92-84, 1992 (unpublished).

[3] H. A. Bethe, Phys. Rev. **66**, 163 (1944).

[4] S. S. Kurennoy, Part. Accel. **39**, 1 (1992).

[5] R. L. Gluckstern, Phys. Rev. A **46**, 1106 (1992); **46**, 1110 (1992).

[6] S. S. Kurennoy and G. V. Stupakov, Part. Accel. **45**, 95 (1994).

[7] S. S. Kurennoy, Phys. Rev. E **55**, 3529 (1997). Please note a typo in Eq. (6) there: the denominator should be ${}_2F_1(1, 1/2; 5/2; 1 - a^2/h^2) - 3$.

[8] G. V. Stupakov and S. S. Kurennoy, Phys. Rev. E **49**, 794 (1994).

[9] S. De Santis, M. Migliorati, L. Palumbo, and M. Zobov, Phys. Rev. E **54**, 800 (1996).

[10] R. L. Gluckstern and A. V. Fedotov, AIP Conf. Proc. **496**, 77 (1999). Please note that Eq. (16) there should have an extra factor β in the right-hand side, as follows from Eqs. (13) and (14) taking into account $k = \omega/(\beta c)$.

[11] R. L. Gluckstern, CERN Yellow Report 2000-011 (2000).

[12] A. M. Al-Khateeb, O. Boine-Frankenheim, I. Hofmann, and G. Rumolo, J. Phys. G **27**, 2471 (2001).

[13] S. S. Kurennoy, Phys. Rev. ST Accel. Beams **2**, 032001 (1999).

[14] R. E. Collin, *Field Theory of Guided Waves* (IEEE Press, New York, 1991).

[15] *Handbook of Accelerator Physics and Engineering*, edited by A. W. Chao and M. Tigner (World Scientific, Singapore, 1999), Sec. 3.2.5, and references therein.

[16] S. S. Kurennoy, physics/0001065.

[17] A. V. Fedotov and R. L. Gluckstern, Phys. Rev. E **54**, 1930 (1996).

[18] S. S. Kurennoy, Phys. Part. Nucl. **24**, 380 (1993).

[19] B. W. Zotter and S. A. Kheifets, *Impedances and Wakes in High-Energy Accelerators* (World Scientific, Singapore, 1998).

[20] MATHEMATICA, version 5.2. Wolfram Research, Inc., see at www.wolfram.com.

[21] S. S. Kurennoy, AIP Conf. Proc. **496**, 361 (1999).

[22] *Higher Transcendental Functions*, edited by A. Erdelyi (McGraw-Hill, New York, 1953), Vol. 2, Chap. 7.